Exploring steam stability of mesoporous alumina species for improved carbon dioxide sorbent design

Matthew E. Potter,[a]φ Jason J. Lee,[a] Lalit A. Darunte,[a] Christopher W. Jones[a]*

[a] Dr. M. E. Potter, J. J. Lee, Dr. L. A. Darunte and Prof. C. W. Jones: School of Chemical & Biomolecular Engineering, Georgia Institute of Technology, 311 Ferst Drive NW, Atlanta, GA, 30332 (USA)

* E-mail: cjones@chbe.gatech.edu

φ Present address for Matthew E. Potter: Department of Chemistry, University of Southampton, Southampton, Hants, SO17 1BJ, UK.

Abstract

Many different metrics exist to assess the efficacy of a carbon capture sorbent, though one of the pivotal characteristics is stability on regeneration, most notably steam stability, which applies to steam stripping regeneration, a technique proposed for capture of CO_2 from humid flue gas. In this study the steam stability of two different mesoporous alumina species is compared, with an aim to tune the synthesis methodology, and the local structure and crystallinity of the samples, to create a stable regenerable sorbent. The roles of calcination temperature and aminopolymer impregnation on sorbent stability and structure are also investigated using a wide range of characterization techniques to specifically probe the influence of the alumina support. We show through this study that support choice, and support stability, can play an important role in sorbent design for carbon capture. We highlight that regular crystallinity (such as in γ-alumina), hinders the formation of pseudo-boehmite, retaining its CO_2 uptake. Further we show that the addition of aminopolymers (PEI) can facilitate phase changes, however maintains the mesoporosity of the sample, a key metric for CO_2 uptake.

Keywords

Alumina, Steam-stability, CO_2 capture, aminopolymer

1. Introduction

One of the primary challenges of an expanding and developing global population is increasing energy demands, where fossil fuels will almost certainly be the primary contributor for the foreseeable future [1]. While finite fossil fuel reserves mean this cannot be sustained indefinitely, the immediate concern is the accompanied generation of greenhouse gases. It is widely known that increasing atmospheric CO_2 concentration is linked to violent weather conditions, and adverse health effects, as such, legislation is being developed to control its emission [2,3]. This has led to a significant rise in the development of carbon capture and sequestration (CCS) techniques.

The current benchmark post-combustion CCS technology employs liquid amines (typically monoethanolamine) to curb CO_2 emissions from power plants, and other industrial point sources, accounting for over 60 % of global CO_2 emissions [4]. While this has been widely implemented for numerous separations (though not post-combustion CO_2 capture), it has several disadvantages. The highly volatile amines lead to sorbent loss and equipment corrosion. Further, significant amounts of energy are needed for regeneration, making the process costly, and less environmentally sustainable [5,6]. As such, a range of solid sorbents (e.g. with advantaged heat-capacities) have been investigated for CCS applications with zeolites [7], MOFs [8], activated carbons [9], alkali earth metals [10] and amine-based solids [11-16] among the most common. Amine-based solids have attracted significant as the combination of a porous support, with tunable amine sites, provides a robust material with strong CO_2 – amine interactions. This facilitates rapid CO_2 uptake, even at low CO_2 concentrations (400 ppm, simulated direct air capture conditions) [3]. As a result, the many different amine-based sorbents have been grouped into four classes, based on how the amine is added to the material: an oligomeric/polymeric species impregnated within the pore (class 1) [17-20], chemically grafted within the pore *via* an organosilane (class 2) [21-23], polymerized *in situ* within the pore (class 3) [24] or a combination of separate oligomeric/polymeric and grafted organosilane species (class 4) [25].

Class 1 aminopolymer-impregnated materials have received a significant amount of attention as the high amine content bestows improved CO_2 uptake [26-28]. Among the most widely researched amimopolymers is poly(ethyleneimine) (PEI), as its larger molecular weight makes it more resistant to leaching, compared to smaller amines [29]. The most common supports for aminopolymers are mesoporous silica and aluminas [30,31], however novel new technologies are rapidly emerging [32,33]. While the majority of literature utilizes silica supports, aluminas have repeatedly been shown to be more thermally and chemically resilient [34,35]. While many studies focus on optimizing the carbon capture properties of these class 1 materials, comparatively few focus on the practical aspects of regeneration or stability [36,37], which are vital to the regeneration process, and for industrial implementation.

Typically aminopolymer systems are regenerated using a combination of pressure, temperature or vacuum swing desorption techniques [38]. Yet recent work has shown the benefits of steam stripping as a regeneration technique [39,40]. Steam stripping can utilize inexpensive, low-value steam that is readily available, making it highly appealing. Direct steaming of sorbents has been shown to facilitate faster CO_2 desorption, as the water disrupts the CO_2-amine interactions [41]. Once the CO_2 is desorbed, the steam is then condensed, leaving a stream of high purity CO_2 for sequestration [42-44]. It is also noted that even if an alternative regeneration technique is used, the flue gas emitted from industrial plants, and other point sources, is not dry, containing between 3 – 10 % H_2O [44]. Thus, regardless of the regeneration technique employed, steam stability is still fundamental to practical sorbent design. Several studies have focused on the stability of the amine species under these simulated steam stripping conditions [41-44]. We have previously shown that amine-functionalized mesocellular foam (MCF) is susceptible to structure degradation on steaming. It was shown that both surface area and pore volume of MCF-PEI greatly reduced from 201 m^2/g and 1.54 cm^3/g to 72 m^2/g and 0.58 cm^3/g after steaming in air for 24 hours [36]. This, in combination with amine loss, led the CO_2 uptake to drop from 1.26 mmol/g to 0.91 mmol/g [36]. However, Choi *et al* suggest that silicas with thicker walls, larger pore volumes and pore diameters could be more resilient to steam stripping. They showed that macroporous silica impregnated with PEI can retain 90 % CO_2 uptake after 14 days of steaming, whereas PEI impregnated MCM-41, SBA-15 and MCF could only retain 38 %, 50 % and 58 % respectively [44]. Despite these studies, few have focused on the stability of the support in isolation.

In our previous work we compared the CO_2 uptake of two different class 2 mesoporous alumina supports [45]. One support was 'ordered', with a crystalline γ-Al_2O_3 structure, with entwinned mesoporous regions, while the other support was 'disordered' with no obvious local structure. The two bare supports had notable differences, with the 'disordered' species possessing strong basic sites, leading to greater CO_2 uptake, and stronger interactions with the support (~ 80 kJ mol^{-1}). In contrast, the ordered support, behaved in a similar fashion to silica. In this study we aim to understand the stability of these two different supports under simulated steam stripping conditions. In doing so we observe the influence of calcination temperature on these supports, to optimize their physico-chemical properties for future sorbent development, using a range of characterization techniques to probe the alumina supports. We also compare the influence of impregnating the supports *prior* to steam stripping, thereby observing the influence of the PEI aminopolymer on structural changes resulting from steam-stripping. We believe this applied study will aid the practical development of CO_2 sorbents, while also being highly relevant to other fields such as catalysis, specifically, aqueous phase reforming, where steam stability is a highly pertinent subject for alumina-supported catalysts [46,47].

2. Materials and Methods

2.1. Chemicals

All chemicals were obtained from Sigma Aldrich and used without further purification.

2.2. Synthesis of ordered mesoporous alumina; OAl

First, 13.80 g of Catapal B alumina was sonicated for 90 min in a solution of 200 mL of deionized water with 0.9 mL of concentrated nitric acid to give a white suspension. This was stirred at 60 ^oC for 18 h. Separately, 15.54 g of P123 was dissolved in 200 mL of ethanol. This was added to the alumina suspension and stirred at room temperature for 24 h. The sample was then synthesized by heating to 60 ^oC in an evaporation dish for 48 h. The resulting yellow sample was dried overnight at 75 ^oC and subsequently calcined at a ramp rate of 1 ^oC/min to either 400,

550, 700 or 900 ^{o}C (as indicated) where it was held for 4 h. This series of species is labelled as "ordered" as it is known to form γ-Al_2O_3, hence form in an ordered fashion [45].

2.3. Synthesis of disordered mesoporous alumina; DAl

First, 20.64 g of P123 was dissolved in 500 mL of ethanol. Once dissolved, 35 mL of concentrated nitric acid was added along with 51.15 g of aluminum isopropoxide. This was stirred vigorously for 5 h at room temperature. The solution was then synthesized by heating to 60 ^{o}C for 48 h. The material was then calcined (without further drying) at 400, 550, 700 or 900 ^{o}C (as indicated) for 4 h, with a ramp rate of 1 ^{o}C/min. This series is labelled as "disordered" as it is not known to be amorphous and not form a specific alumina phase [45].

2.4. PEI Impregnation

Initially, 1.0 g of mesoporous alumina was stirred with 15 mL of methanol at room temperature for 1 hour. A 20 mL solution of methanol containing either 670 mg of 800 MW branched poly(ethyleneimine) was added to the slurry to achieve 40 wt% of PEI and stirred for a further 24 hours at room temperature. The solvent was then removed under reduced vacuum at 50 ^{o}C to yield a powder. The sample was then dried at 110 ^{o}C for 12 hours at 10 mbar. Samples impregnated with PEI are labelled with "PEI".

2.5. Simulated steam stability

Typically, 0.3 g of powder was placed into a Teflon holder, covered with a metal frit, designed to allow water vapor through, but not liquid water. The Teflon holder was placed into an autoclave with 20 mL of water, purged with nitrogen thrice, and heated to 120 ^{o}C for 20 h. The powder was then removed and dried under 10 mbar of vacuum at 110 ^{o}C for 12 h. Samples that have been steamed are labelled with "St".

2.6. Powder X-ray diffraction (XRD)

Powder XRD patterns were obtained by use of a PANalytical X'pert diffractometer with a Cu Kα X-ray source.

2.7. Organic content

The organic content of the samples was estimated using a Netzsch STA409PG TGA. Weight loss was calculated from the mass loss between 120 to 900 ºC, under a combined flow of 90 mL/min of air and a 30 mL/min of nitrogen. The data were collected between 25 and 900 ºC heating at a rate of 10 ºC/min.

2.8. Physisorption

Nitrogen physisorption was performed on a Micrometrics Tristar 3020 instrument at 77 K. Samples were degassed for 12 hours at 110 ºC prior to analysis. Surface area was calculated using the BET model. Pore volumes and pore-size distributions were calculated using the Bdb-FHH model [48].

2.9. CO_2 capacity measurements

CO_2 capacities were measured using a TA instruments Q500 TGA. Samples were pretreated under a 100 mL/min flow of helium at 110 ºC for 3 hours. The sorbent uptake was then measured from the gain in mass after subsequent exposure to 10 % CO_2 in helium at 30 ºC, flowed at 90 mL/min for 6 h, with a 10 mL/min balance helium flow.

2.10. ^{27}Al MAS NMR

^{27}Al cross-polarization magic angle spinning (CP-MAS) solid-state nuclear magnetic resonance (NMR) measurements were carried out on a Bruker DSX-300 spectrometer. The samples had been exposed to atmospheric conditions (non-dehydrated) and were spun at a frequency of 10 kHz, and 1024 scans were taken.

3. Results and discussions

3.1. Bare supports

The bare mesoporous alumina supports (ordered: OAl and disordered: DAl) were each calcined at 4 different temperatures (400, 550, 700 and 900 ^{o}C) to optimize their textural and physicochemical properties. The crystallinity of the systems, post calcination, was assessed using powder XRD (Fig. S1). The ordered system (OAl, Fig. S1a) shows only broad peaks at 37 and 47 ^{o}, the (311) and (400) signals, respectively for poorly crystalline γ-Al_2O_3 [21,45,49]. The peak intensity grows with increasing calcination temperature, with a peak at 39 ^{o} visible when calcined above 700 ^{o}C. In contrast, calcining the disordered system (DAl, Fig. S1b) below 900 ^{o}C results in no significant features in the pattern. This confirms the lack of crystallinity in the system. However, on calcining at 900 ^{o}C (DAl900), γ-Al_2O_3 signals appear, showing that at higher temperatures the disordered system undergoes a phase change. We note that this observation differs from commercial samples, however this is attributed to the presence of mesopores influencing the surface chemistry.

Thermogravimetric analysis (TGA) combined with differential scanning calorimetry (DSC) gives us greater insight into the systems (Fig. S2). Both OAl400 and DAl400 show a noticeable decrease in mass around 500 ^{o}C, which is also seen *via* DSC. These are attributed to residual organic species that were not removed on calcination at 400 ^{o}C. For the ordered series (OAl, Fig. S2a) the combustible content decreases with increased calcination temperature, likely due to the dehydration of hydroxyl species. In contrast, DAl550 (Fig. S2b) has greater combustible mass than DAl400. For DAl550, the majority of the mass is lost in the 120 – 300 ^{o}C regime, which is likely due to the sorption of atmospheric species onto its strongly basic sites [45,50], or due to large quantities of surface hydroxyl species on removing the organic components. However, given the total mass lost is around 14 wt%, it is unlikely that this is purely due to the removal of hydroxyl species.

N_2 physisorption (Fig. S3) shows all systems have a type IV hysteresis, with mesoporosity and limited microporosity, in line with our previous findings [45]. The OAl series (Fig. S4) shows a linear decrease in surface area with calcination temperature, whereas the pore volume remains

constant. Further the pore-size distributions (Fig. S5) show that the average pore size of the OAl materials increases, with a less uniform distrbution, as the calcination temperature increases (Fig. S5a). Reduction in surface area occurs as the pores become increasingly irregular, and can be attributed to sintering and the collapse of particles leading to larger pores [51]. In contrast, the pore volume and surface area of the DAl series reach a maximum for DAl-550 (Fig. S4), but decreases past this temperature. Here the pore size distribution appears to narrow, with the average pore diameter decreasing with increased calcination temperature (Fig. S5b). The initial increase in porosity is likely due to structural changes, as the combustible content of the DAl400 species is removed, clearing the pores and increasing the surface area and pore volume. However, beyond 550 ºC, densification occurs as the phase change to γ-Al_2O_3 ensues. We note in both cases the pore distribution is not smooth, as expected in SBA-15, but is rougher, this is in line with our previous work on alumina samples [45].

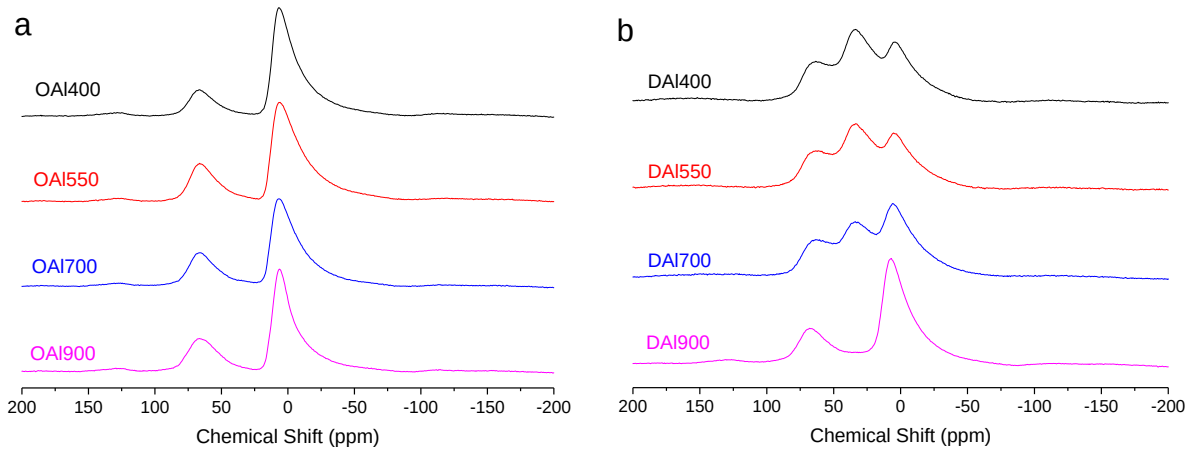

Fig. 1 Solid state MAS ^{27}Al NMR of bare, ordered (OAl, a) and bare, disordered (DAl, b) alumina species as a function of the original calcination temperature of the alumina. The spectra have been offset for clarity

^{27}Al MAS NMR was employed to probe the local structure of the alumina (Fig. 1). The ordered; OAl series shows two defined peaks at 66 and 6 ppm, in a 1:3 ratio, attributed to tetrahedral AlO_4 and octahedral AlO_6 respectively (Fig. 1a), in good agreement with γ-Al_2O_3 [21,45,49]. Increasing the calcination temperature, increases the relative intensity of the tetrahedral signal, and a feature at 35 ppm appears. This feature is attributed to Al_V, formed by dehydrating hydroxyl groups in γ-Al_2O_3, a known Lewis base site [52]. Thus, increasing the calcination

temperature promotes lower coordinated aluminum, due to dehydration. DAl400 (Fig. 1b) shows three signals at 66, 35 and 4 ppm, again attributed to octahedral, pentacoordinate surface sites and tetrahedral aluminum respectively. As the calcination temperature increases, the pentacoordinate signal decreases as the octahedral species increases, showing a change from 5 to 6 coordinated aluminum. Once the calcination temperature reaches 900 ºC (DAl900), the system resembles γ-Al_2O_3, in good agreement with XRD findings (Fig. S1).

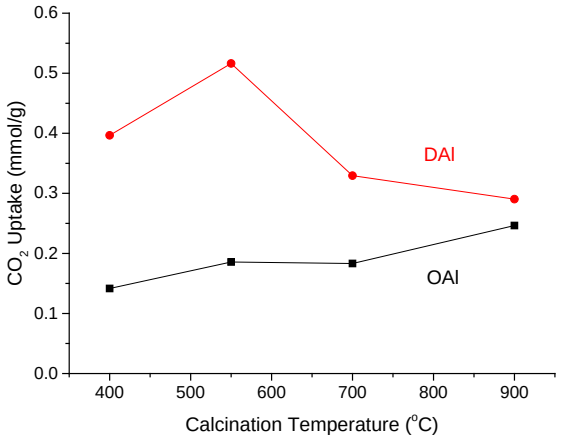

Fig. 2 CO_2 uptake of the bare, ordered (OAl, black) and bare, disordered (DAl, red) alumina, as a function of the original calcination temperature of the alumina. CO_2 uptake measurements were done at 30 ºC, with dry 10 % CO_2 in helium

The CO_2 uptake of the bare supports show distinct trends for the two-different series (Fig. 2). The CO_2 uptake of the OAl series increases as the calcination temperature increases, despite the reduced surface area (Fig. S4). This is likely due to the appearance of strong Lewis base, Al_V sites, seen by ^{27}Al NMR (Fig. 1a), that would interact strongly with CO_2, leading to a higher uptake for the bare support [45,50]. The DAl series adsorbs notably more CO_2 than the OAl series, mirroring trends in our previous work [45], which were attributed to the presence of a large proportion of strongly basic O^{2-} species, capable of forming carbonates. The CO_2 uptake follows a similar trend to the pore volume and surface area, peaking at DAl550, and then decreasing. This suggests that porosity is the key factor in CO_2 sorption, as a greater surface area and pore volume improves the sorbents uptake behavior.

3.2. Steaming of bare supports

The mesoporous alumina sorbents were then treated under simulated steam stripping conditions to investigate their stability, and suitability, for practical regeneration [39,40]. Powder XRD shows only subtle differences between the steamed (St-OAl) and fresh (OAl) series (Fig. S6), as features emerge at 39 and 49 °, suggesting a small quantity of pseudo-boehmite has formed [53-55]. The pore volume, surface area (Fig. 3a & S7), pore-size distribution (Fig. 3b) and TGA data (Fig. S8) showed the steamed samples (St-OAl) were similar to the fresh samples (OAl). The ^{27}Al NMR spectra were also similar (Fig. 3b), though, the Al_V feature in the ^{27}Al MAS NMR (36 ppm) is no longer visible, likely it has been rehydrated to octahedral alumina. Overall this suggests the OAl series is relatively resilient to the simulated steam stripping conditions used.

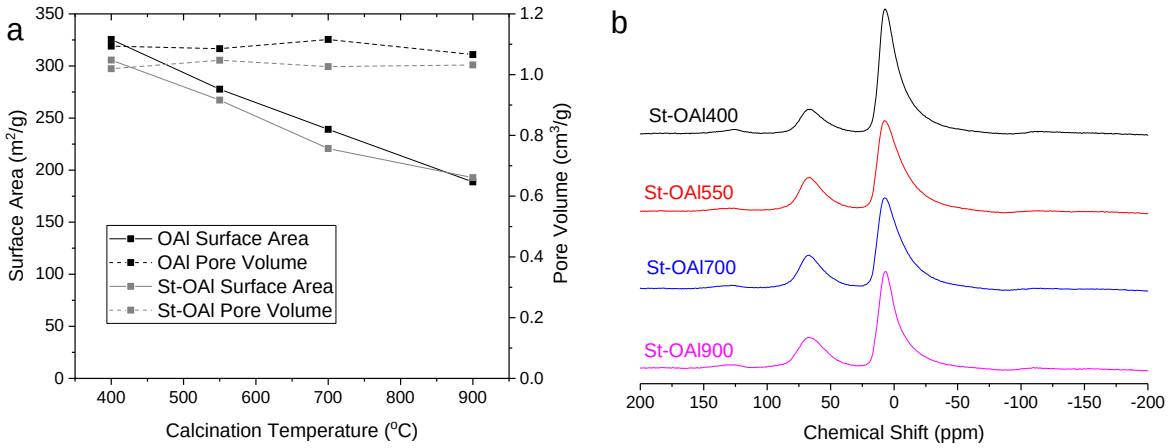

Fig. 3 a) The variation in surface area (solid lines) and pore volume (dashed lines) of bare ordered alumina (OAl, black) and after steaming (St-OAl, grey) as a function of the original calcination temperature of the alumina. b) Solid state MAS ^{27}Al NMR of steamed, bare, ordered (St-OAl) as a function of the original calcination temperature of the alumina. The spectra have been offset for clarity

In contrast, the DAl series undergoes substantial changes on steaming, as St-DAl400, St-DAl550 and St-DAl700 have a significant pseudo boehmite contribution (Fig. S9) [53-55]. However, St-DAl900 is similar to the original DAl900 pattern, with only small contribution from pseudo boehmite at 49 °. This suggests DAl900 was more resistant to steaming, likely due to the robust, crystalline γ-Al_2O_3 present.

N_2 physisorption shows that St-DAl400, St-DAl550 and St-DAl700 a now have a type III isotherm, with some residual porosity (Fig. S10a), as the surface areas and pore volumes reduced after steaming (Fig. 4a). Here, systems with pseudo boehmite present have greatly reduced pore volumes and surface areas, attributed to the dense nature of pseudo-bohemite [53]. However, the values St-DAl900 and DAl900 are comparable, suggesting little framework degradation has occurred. Again, the γ-Al_2O_3, formed on calcining at higher temperatures, likely makes the material more resistant to steaming (as previously seen in the St-OAl series), allowing the system to retain its physicochemical characteristics.

In the DAl series, the trends of surface area versus calcination temperature are reversed on steaming, as St-DAl550 is now a minimum (Fig. 4). This is also attributed to pseudo boehmite formation, which primarily occurs on the alumina surfaces via hydroxylation [53-55]. The more surface area available, the faster the rate of hydroxylation, leading to a greater proportion of dense phase material [53-55]. The pore size distribution (Fig. S10b) shows only St-DAl900 maintains mesoporosity (similar to DAl900). In contrast, the other three St-DAl samples present a featureless line, suggesting any porosity is highly disordered, again due to the structural changes on pseudo boehmite formation.

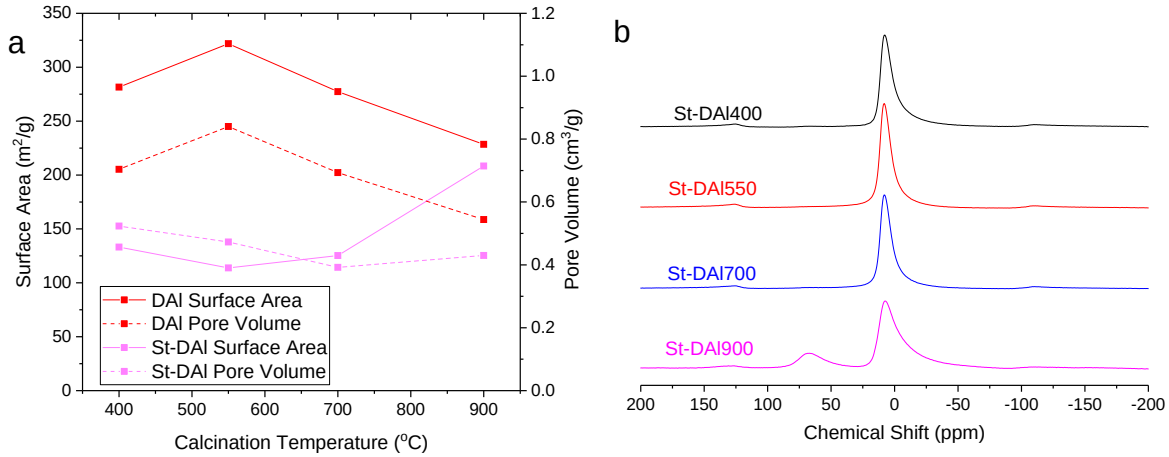

Fig. 4 a) The variation in surface area (solid lines) and pore volume (dashed lines) of bare disordered alumina (DAl, red) and after steaming (St-DAl, pink) as a function of the original calcination temperature of the alumina. b) Solid state MAS ^{27}Al NMR of steamed, bare, disordered (St-DAl) as a function of the original calcination temperature of the alumina. The spectra have been offset for clarity

TGA (Fig. S11) and NMR (Fig. 4b) also show pseudo boehmite formation. St-DAl400, St-DAl550 and St-DAl700 show a greater weight loss than the pre-steamed samples, and St-DAl900, due to the dehydration of the pseudo boehmite (AlOOH) to alumina (Al_2O_3) at elevated temperatures. However, there is also likely to be some adsorbed water and defect surface species present in steamed samples, explaining the larger weight loss. The DSC (Fig. S11) also highlights the difference in the two structures, with a signal at 400 ^oC, attributed to the dehydration of pseudo boehmite. St-DAl900 shows only a subtle signal at 450 ^oC, due to the small quantity of pseudo boehmite formed (as seen by powder XRD, Fig. S9). The NMR data (Fig. 4b) are in good agreement with these findings, as St-DAl900 resembles the unsteamed DAl900, whereas the other three samples presenting a single signal attributed to octahedral AlO_6 at 7 ppm, typical of pseudo boehmite [53-55]. The lack of tetrahedral Al signal (60 – 70 ppm) suggests that pseudo boehmite is now the dominant phase in the sample [53-55].

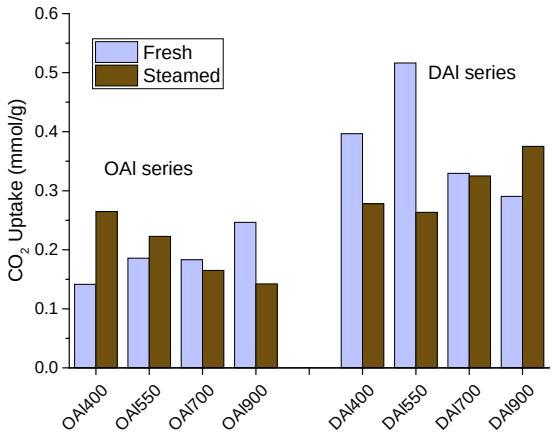

Fig. 5 CO_2 uptake of the bare, ordered (OAl, left) and bare, disordered (DAl, right) series for fresh samples (pale blue), and after steaming (brown), as a function of the original calcination temperature of the alumina. CO_2 uptake measurements were made at 30 ^oC, with dry 10 % CO_2 in helium

The CO_2 uptake of both sets of steamed supports differed from the fresh series (Fig. 5). Fresh OAl showed a higher CO_2 uptake when calcined at higher temperature, attributed to the dehydration of octahedral species to form strong Lewis base Al_V defect sites, capable of interaction with CO_2 [45]. The reverse trend is seen on steaming, with the St-OAl series showing higher CO_2 uptake for samples with lower original calcination temperature, following the same

trend as the surface area. This is likely because steaming over 24 hours saturated the surface with hydroxyl species that can bind to CO_2 [56]. Thus, a higher surface area means more hydroxyl groups, correlating with a greater CO_2 uptake. The CO_2 uptake of the disordered (DAl) series also follows the same trend as surface area, again likely due to hydroxyl formation on the surface after steaming.

3.3. PEI-Impregnated Supports

The steam stability of PEI impregnated aluminas was investigated, with the supports (calcined at different temperatures) impregnated with PEI, and then steamed. The powder XRD patterns of the PEI impregnated OAl series (PEI-OAl, Fig. 6a) agree with the undoped bare OAl species (Fig. S1a), showing just γ-Al_2O_3 features. On steaming the PEI-OAl series, features attributed to pseudo boehmite emerge, for all samples except St-PEI-OAl900, which again appears to be resilient (Fig. 6a). Contrasting the St-OAl and St-PEI-OAl series shows PEI-impregnated species contain more pseudo boehmite. Thus, the amines in PEI may accelerate pseudo boehmite formation on steaming. The steaming of PEI-DAl (Fig. 6b) results in the significant formation of pseudo boehmite in St-PEI-DAl400, St-PEI-DAl550 and St-PEIDAl700. Previously St-DAl900 retained its γ-Al_2O_3 features (Fig. S9); however, again it appears the inclusion of PEI has accelerated the formation of pseudo boehmite, as these features are now prominent in St-PEI-DAl900 (Fig. 6b).

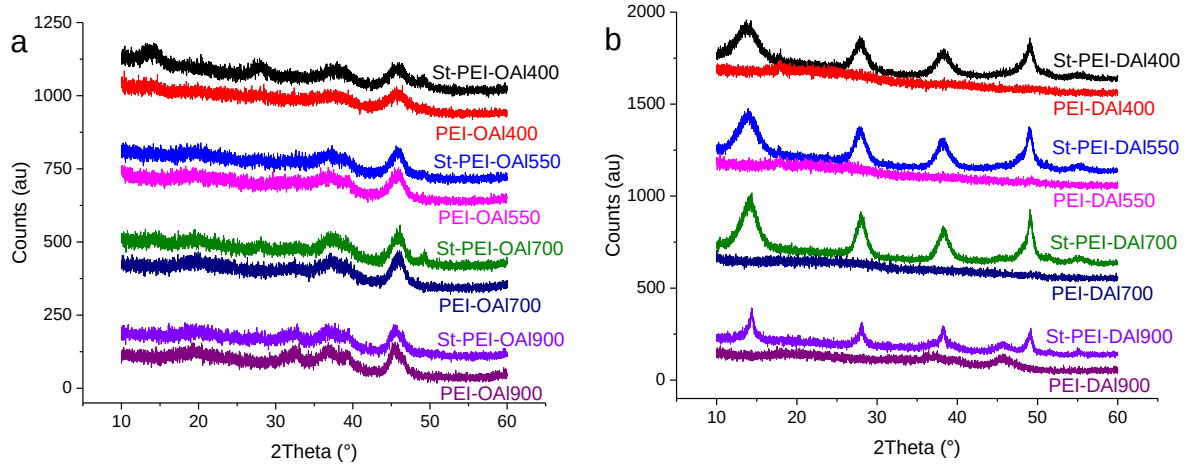

Fig. 6 Wide angle powder XRD patterns of a) PEI-impregnated, ordered alumina, both before (PEI-OAl) and after steaming (St-PEI-OAl) and b) PEI-impregnated, disordered alumina, both before (PEI-DAl) and after steaming (St-PEI-DAl) as a function of the original calcination temperature of the alumina. The patterns in are offset by 75 counts in a, 100 counts in b, between fresh and steamed samples, with different calcination temperatures offset by 300 counts in a, 500 counts in b, for clarity

TGA data quantified the PEI loading in the impregnated samples (Fig. S12 & S13). For both the PEI-OAl and PEI-DAl series, the amine loading was found to be 9 – 13 mmol of amine/g of alumina (Fig. S12a & S13a). Previous literature shows there is minimal leaching under simulated steam conditions, thus, the amine loading is not expected to vary significantly, post-steaming, in these systems [40,41]. However changes in our TGA data on steaming PEI-containing species (Fig. S12b & S13b) could be due to many factors, including strongly-bound water, hydroxyl formation, amine degradation, etc. [1], meaning accurate comparisons cannot be made based purely on the support. Again steamed St-PEI-DAl (Fig. S13b) series shows a greater weight loss than fresh PEI-DAl (Fig. S13a), partially due to pseudo boehmite formation. The DSC data in all cases was dominated by a signal at 200 ^{o}C, not seen in the bare supports, attributed to the presence of PEI. However, no notable variations could be solely attributed to the support for the PEI-containing samples, regardless of steaming, or alumina type.

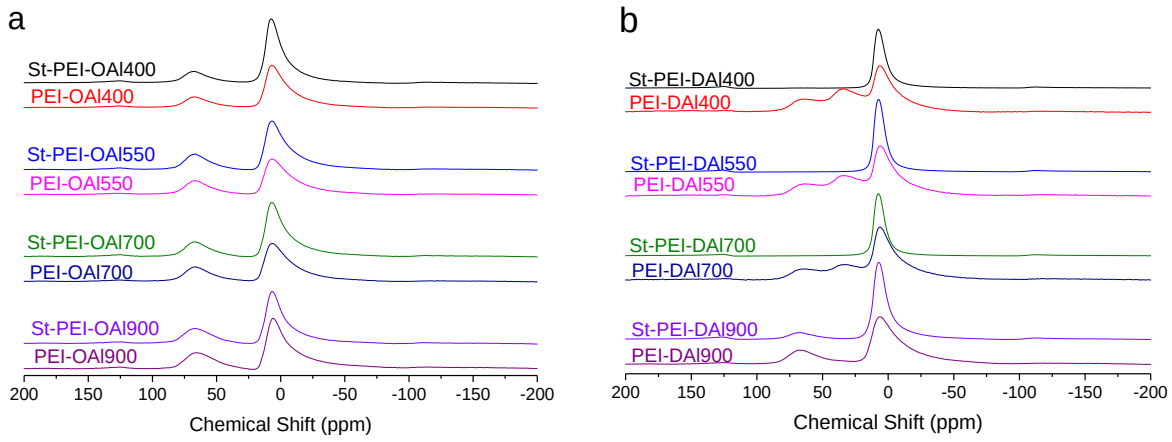

Fig. 7 Solid state MAS ^{27}Al NMR of a) PEI-impregnated, ordered alumina, before (PEI-OAl) and after steaming (St-PEI-OAl), and b) PEI-impregnated, disordered alumina, before (PEI-DAl)

and after steaming (St-PEI-DAl) as a function of the original calcination temperature of the alumina. The spectra have been offset for clarity and ease of comparison

^{27}Al MAS NMR shows little differences between the St-PEI-OAl and PEI-OAl series, (Fig. 7a) as both show a tetrahedral AlO_4 signal at 68 ppm, and an intense octahedral AlO_6 signal at 7 ppm, in a 1:3 ratio, akin to the bare OAl series (Fig. 3b). The only subtle difference is St-PEI-OAl900 has a greater proportion of octahedral sites than PEI-OAl900, likely due to the pseudo boehmite formation. The PEI-DAl series (Fig. 7b) is similar to the bare DAl series (Fig. 4b), except the Al_V site at 33 ppm is less intense on PEI impregnation, likely due to the interaction between PEI and the basic sites, converting the Al_v sites to octahedral aluminum, overlapping with the AlO_6 signal. Again on steaming the PEI-DAl series the first three samples suggest pseudo boehmite is the dominant phase (Fig. 7b), with just one peak present at 7 ppm, representing octahedral alumina. Comparing St-PEI-OAl900 (Fig. 7a) with St-OAl900 (Fig. 3b) shows the former has a larger proportion of octahedral Al, whereas the latter is closer to the expected 1:3 ratio, typical of γ-Al_2O_3. This again is due to the amine groups of the PEI accelerating the formation of pseudo boehmite.

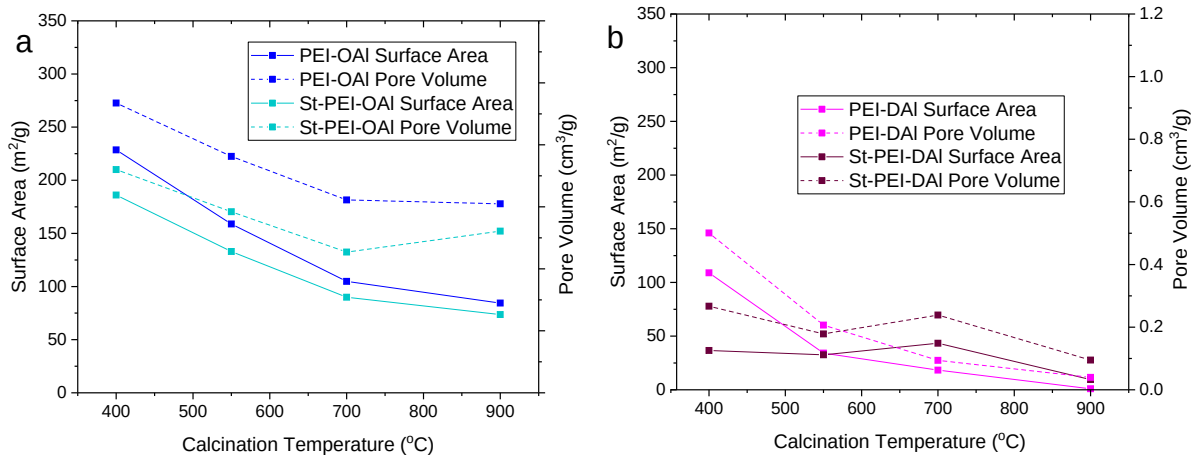

Fig. 8 Showing the variation in surface area (solid lines) and pore volume (dashed lines) of a) PEI-impregnated, ordered alumina, before (PEI-OAl, blue) and after steaming (St-PEI-OAl, cyan) and b) PEI-impregnated, disordered alumina, before (PEI-DAl, magenta) and after steaming (St-PEI-DAl, purple) as a function of the original calcination temperature of the alumina

Physisorption data of the PEI-OAl series shows a decrease in pore volume and surface area on introducing PEI (Fig. 8a), causing a narrower pore distribution (Fig. S14b), and lower average pore dimeter, as PEI coats the walls of the mesopores, as seen in SBA-15 [58]. On steaming, the PEI-OAl series maintains its porosity (St-PEI-OAl), showing only slight variation in isotherms (Fig. S14a) and pore-size distributions (Fig. S14b). This is in good agreement with powder XRD (Fig. 6a) and ^{27}Al NMR findings (Fig. 7a), showing the resilience of the ordered alumina. The surface areas and pore volumes of PEI-OAl decrease on steaming (Fig. 8a), due to pseudo boehmite formation, as seen in the XRD.

Impregnation of PEI into the DAl series (PEI-DAl) also reduced pore volume and surface area (Fig. 8b). Further, the inclusion of PEI results causes differences in the support behavior on steaming. The N_2 isotherms of both the PEI-DAl and St-PEI-DAl show a type IV isotherm (Fig. S15), whereas St-DAl had a type III isotherm (Fig. S10a). This suggests PEI helps maintain the porosity. This can also be seen in the pore-size distributions, where the PEI-DAl maintains a similar pore-size distribution as the DAl system (Fig. 9). When PEI was absent, there was no signs of mesoporosity after steaming (St-DAl), whereas all St-PEI-DAl samples do show mesoporosity is present after steaming. The PEI may act like a template, preserving the mesopores around it, therefore polymeric/oligomeic species could create defined mesoporosity, serving as steam stable CO_2 sorbents. However, the surface areas and pore volumes of PEI-DAl still decrease on steaming, again attributed to the formation of dense-phase pseudo boehmite as seen in the XRD pattern (Fig. 8b).

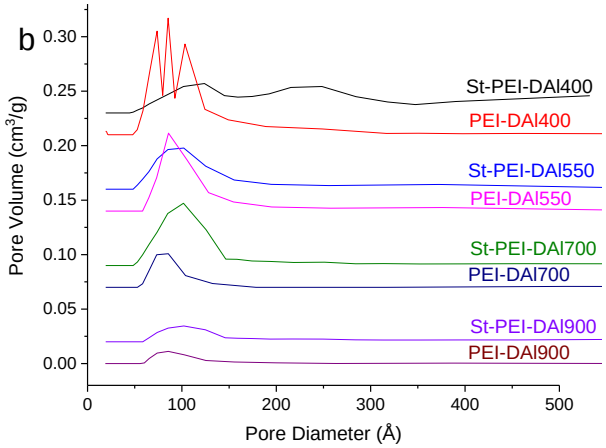

Fig. 9 Pore size distributions analyzed by the BdB-FHH method of fresh PEI-impregnated disordered alumina (PEI-DAl), and after steaming (St-PEI-DAl). The distributions are offset by 0.02 cm^3/g between analogous fresh and steamed samples, and by 0.07 cm^3/g between the original alumina calcination temperatures, for clarity

The PEI impregnated systems were tested for CO_2 uptake under simulated flue gas conditions, comparing fresh species with steamed (Fig. 10). The CO_2 uptake is improved considerably on PEI impregnation, due to available amine sites. The PEI-DAl and PEI-OAl able to maintain their CO_2 uptakes on steaming; in most cases, the capacity varies by less than 5 %. Two notable exceptions to this are PEI-OAl700 and PEI-DAl700. The onset of pseudo boehmite is most pronounced for St-PEI-OAl700 in the St-PEI-OAl series, with a peak clearly visible at 49 º. The associated changes in surface chemistry is the most likely the cause of the reduced CO_2 uptake, with dense phase pseudo boehmite limiting CO_2 diffusion, blocking access to the amine sites in PEI. The other distinct deviation, St-PEI-DAl700, is likely the result of a change in porosity. Both surface area and pore volume in St-PEI-DAl700 are notably higher than the rest of the series, and also higher than PEI-DAl700. The improvements to the surface area on steaming may alter the morphology of the PEI, or improve CO_2 diffusion, allowing more amine sites to interact with the CO_2. To further emphasize the importance of surface area and pore volume for PEI-impregnated species, comparing the amine efficiencies of the fresh samples (PEI-OAl and PEI-DAl) shows the amines are more effective CO_2 sorbents in PEI-OAl (Fig. S16). This is likely due to the higher surface areas and pore volumes of the PEI-OAl series compared to PEI-DAl. We note in all cases the amine efficiency is less than 25 %, which is below the theoretical maximum of 39 % for these branched PEI samples (4:3:2 of 1º:2º:3º amines), suggesting the PEI is operating below maximum efficiency.

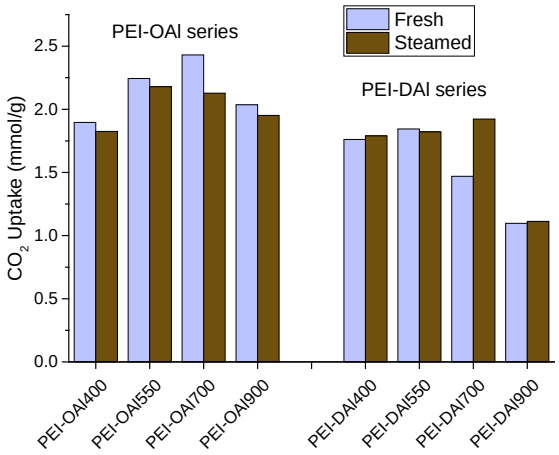

Fig. 10 CO_2 uptake of the PEI-impregnated, ordered (PEI-OAl, left) and PEI-impregnated, disordered (PEI-DAl, right) series for fresh samples (pale blue), and after steaming (brown), as a function of the original calcination temperature of the alumina. CO_2 uptake measurements were made at 30 ^oC, with dry 10 % CO_2 in helium

4. Conclusions

To effectively design CO_2 sorbents, a wide range of criteria must be satisfied, including the practical regeneration of the sorbent. While the benefits of different regeneration techniques are being debated for amine-containing sorbents, steam stability is crucial for steam-stripping regeneration, and is a vital for CO_2 adsorption for flue gas sorption from industrial point sources. As such, mesoporous alumina is a viable support for amine-based sorbents, given the stability of the system. By comparing a range of alumina supports, we have shown that local crystallinity, such as γ-Al_2O_3, improves steam stability, by preventing the formation of pseudo boehmite, which limits the CO_2 uptake of the bare sorbent. In light of this, we demonstrate that steam stripping can have a significant influence on the nature of framework sites for CO_2 sorption. Namely, the rehydration of coordinatively unsaturated alumina sites in the ordered alumina, which was found to hinder CO_2 uptake. However, once hydrated through steaming, the uptake of the alumina sample is directly linked to the porosity of the sample, where species with high surface areas and pore volumes show the best CO_2 uptake behavior. This is likely the result of the surface becoming saturated with surface hydroxyl species. Further we show that while the amine sites of PEI drastically improve the CO_2 uptake, they can facilitate the transformation of

the alumina structure to pseudo boehmite. However, in spite of this, the aminopolymer is also able to act as a template, forcing the alumina to retain its mesoporosity on steaming, resulting in pseudo boehmite with defined mesopores. Overall, we have probed the complex behavior of alumina supports, and their stability towards steam. We believe that this work has offers practical insights towards designing improved CO_2 sorbents for flue gas capture.

5. Funding Sources

This work was supported by the Center for Understanding and Control of Acid Gas-Induced Evolution of Materials for Energy (UNCAGE-ME), an Energy Frontier Research Center, funded by U.S. Department of Energy (US DoE), Office of Science, Basic Energy Sciences (BES) under Award DE-SC0012577.

6. References

[1] Choi S, Gray ML and Jones CW (2011) Amine-tethered solid adsorbents coupling high adsorption capacity and regenerability for CO_2 capture from ambient air, ChemSusChem 4:628-635.

[2] Bonan CB (2008) Forests and Climate Change: Forcings, Feedbacks and the Climate Benefits of Forests, Science 320:1444-1449.

[3] Sanz-Perez ES, Murdock CR, Didas SA and Jones CW (2016) Direct Capture of CO_2 from Ambient Air, Chem Rev 116:11840-11876.

[4] *IEA.* (2012) *CO_2 emissions from fuel combustion Highlights*; OECD/IEA: Paris.

[5] Fisher JC and Gray M (2015) Cyclic stability testing of aminated-silica solid sorbent for post-combustion CO_2 capture, ChemSusChem 8: 452-455.

[6] Wang Q, Luo J, Zhong Z and Borgna A (2011) CO_2 capture by solid adsorbents and their applications: current status and new trends, Energy Environ Sci 4: 42-55.

[7] Bae TH, Hudson MR, Mason JA, Queen WL, Dutton JJ, Sumida K, Micklash KJ, Kaye SS, Brown CM and Long JR (2013) Evaluation of cation-exchanged zeolite adsorbents for post-combustion carbon dioxide capture, Energy Environ Sci 6:128-138.

[8] Fracaroli AM, Furukawa H, Suzuki M, Dodd M, Okajima S, Gandara F, Reimer JA and Yaghi OM (2014) Metal–Organic Frameworks with Precisely Designed Interior for Carbon Dioxide Capture in the Presence of Water, J Am Chem Soc 136:8863-8866.
[9] Chai SH, Liu ZM, Huang K, Tan S and Dai S (2016) Amine Functionalization of Microsized and Nanosized Mesoporous Carbons for Carbon Dioxide Capture, Ind Eng Chem Res 55:7355-7361.
[10] Wang S, Yan S, Ma X and Gong J (2011) Recent advances in capture of carbon dioxide using alkali-metal-based oxides, Energy Environ Sci 4: 3805-3819.
[11] Sayari A and Belmabkhout Y (2010) Stabilization of Amine-Containing CO_2 Adsorbents: Dramatic Effect of Water Vapor, J Am Chem Soc 132:6312-6314.
[12] Dutcher B, Fan M and Russell AG (2015) Amine-Based CO_2 Capture Technology Development from the Beginning of 2013—A Review, ACS Appl Mater Interfaces 7:2137-2148.
[13] Goeppert A, Czaun M, May RB, Prakash GKS, Olah GA and Narayanan SR (2011) Carbon Dioxide Capture from the Air Using a Polyamine Based Regenerable Solid Adsorbent, J Am Chem Soc 133:20164-20167.
[14] Sanz R, Calleja G, Arencibia A and Sanz-Perez ES (2015) CO_2 capture with pore-expanded MCM-41 silica modified with amino groups by double functionalization, Microporous Mesoporous Mater 209:165-171.
[15] Wang XX, Ma XL, Schwartz V, Clark JC, Overbury SH, Zhao SQ, Xu XC and Song C (2012) A solid molecular basket sorbent for CO_2 capture from gas streams with low CO_2 concentration under ambient conditions, Phys Chem Chem Phys 14:1485-1492.
[16] Son WJ, Choi JS and Ahn WS (2008) Adsorptive removal of carbon dioxide using polyethyleneimine-loaded mesoporous silica materials, Microporous Mesoporous Mater 113:31-40.
[17] Wang D, Ma X, Sentorun-Shalaby C and Song C (2012) Development of Carbon-Based "Molecular Basket" Sorbent for CO_2 Capture, Ind Eng Chem Res 51:3048-3057.
[18] Heydari-Gorji A, Belmabkhout Y and Sayari A (2011) Polyethylenimine-Impregnated Mesoporous Silica: Effect of Amine Loading and Surface Alkyl Chains on CO_2 Adsorption, Langmuir 27:12411-12416.

[19] Choi W, Min K, Kim C, Ko YS, Jeon J, Seo H, Park YK and Choi M (2016) Epoxide-functionalization of polyethyleneimine for synthesis of stable carbon dioxide adsorbent in temperature swing adsorption, Nature Commun 7:12640.
[20] Niu MY, Yang HM, Zhang XC, Wang YT and Tang AD (2016) Amine-Impregnated Mesoporous Silica Nanotube as an Emerging Nanocomposite for CO_2 Capture, ACS Appl Mater Interface 8:17312-17320.
[21] Bali S, Leisen J, Foo GS, Sievers C and Jones CW (2014) Aminosilanes Grafted to Basic Alumina as CO_2 Adsorbents—Role of Grafting Conditions on CO_2 Adsorption Properties, ChemSusChem 7:3145-3156.
[22] Zheng F, Tran DN, Busche BJ, Fryxell GE, Addleman RS, Zemanian TS and Aardahl CL (2005) Ethylenediamine-Modified SBA-15 as Regenerable CO_2 Sorbent, Ind Eng Chem Res 44:3099-3105.
[23] Zelenak V, Skrinska M, Zukal A and Cejka J (2018) Carbon dioxide adsorption over amine modified silica: Effect of amine basicity and entropy factor on isosteric heats of adsorption, Chem Eng J 348:327-337.
[24] Drese JH, Choi S, Lively RP, Koros WJ, Fauth DJ, Gray ML and Jones CW (2009) Synthesis–Structure–Property Relationships for Hyperbranched Aminosilica CO_2 Adsorbents, Adv Funct Mater 19:3821-3832.
[25] Wilfong WC, Kail BW, Jones CW, Pacheco C and Gray ML (2016) Spectroscopic Investigation of the Mechanisms Responsible for the Superior Stability of Hybrid Class 1/Class 2 CO_2 Sorbents: A New Class 4 Category, ACS Appl Mater Interfaces 8:12780-12791.
[26] Fujiki J, Chowdbury FA, Yamada H and Yogo K (2017) Highly efficient post-combustion CO_2 capture by low-temperature steam-aided vacuum swing adsorption using a novel polyamine-based solid sorbent, Chem Eng J 307:273-282.
[27] Hammache S, Hoffman JS, Gray ML, Fauth DJ, Howard BH and Pennline HW (2013) Comprehensive Study of the Impact of Steam on Polyethyleneimine on Silica for CO_2 Capture, Energy Fuels 27:6899-6905.
[28] Li KM, Jiang JG, Tian SC, Yan F and Chen XJ (2015) Polyethyleneimine–nano silica composites: a low-cost and promising adsorbent for CO_2 capture, J Mater Chem A 3:2166-2175.
[29] Zhao W, Zhang Z, Li Z and Cai N (2013) Investigation of Thermal Stability and Continuous CO_2 Capture from Flue Gases with Supported Amine Sorbent, Ind Eng Chem Res 52:2084-2093.

[30] Sakwa-Novak MA, Yoo CJ, Tan S, Rashidi F and Jones CW (2016) Poly(ethylenimine)-Functionalized Monolithic Alumina Honeycomb Adsorbents for CO_2 Capture from Air, ChemSusChem 9:1859-1868.
[31] Ebner AD, Gray ML, Chisholm NG, Black QT, Mumford DD, Nicholson MA and Ritter JA (2011) Suitability of a Solid Amine Sorbent for CO_2 Capture by Pressure Swing Adsorption, Ind Eng Chem Res 50:5634-5641.
[32] Mane S, Gao ZY, Li YX, Liu XQ, and Sun LB (2018) Rational Fabrication of Polyethylenimine-Linked Microbeads for Selective CO_2 Capture, Ind Eng Chem Res 57:250-258.
[33] Zhou Z, Balijepalli SK, Nguyen-Sorenson AHT, Anderson CM, Park JL and Stowers KJ (2018) Steam-Stable Covalently Bonded Polyethylenimine Modified Multiwall Carbon Nanotubes for Carbon Dioxide Capture, Energy Fuels 32:11701-11709.
[34] Sakwa-Novak MA and Jones CW (2014) Steam Induced Structural Changes of a Poly(ethylenimine) Impregnated γ-Alumina Sorbent for CO_2 Extraction from Ambient Air, ACS Appl Mater Interfaces 6:9245-9255.
[35] Gunathilake C, Gangoda M and Jaroniec M (2016) Mesoporous Alumina with Amidoxime Groups for CO_2 Sorption at Ambient and Elevated Temperatures, Ind Eng Chem Res 55:5598-5607.
[36] Li W, Bollini P, Didas SA, Choi S, Drese JH and Jones CW (2010) Structural Changes of Silica Mesocellular Foam Supported Amine-Functionalized CO_2 Adsorbents Upon Exposure to Steam, ACS Appl Mater Interfaces 2:3363-3372.
[37] Isenberg M and Chaung SSC (2013) The Nature of Adsorbed CO_2 and Amine Sites on the Immobilized Amine Sorbents Regenerated by Industrial Boiler Steam, Ind Eng Chem Res 52:12530-12539.
[38] Drage TC, Arenillas A, Smith KM and Snape CE (2008) Thermal stability of polyethylenimine based carbon dioxide adsorbents and its influence on selection of regeneration strategies, Microporous Mesoporous Mater 116:504-512.
[39] Li W, Choi S, Drese JH, Hornbostel M, Krishnan G, Eisenberger PM and Jones CW (2010) Steam-stripping for regeneration of supported amine-based CO_2 adsorbents, ChemSusChem 3:899-903.

[40] Chaikittisilp W, Kim HJ and Jones CW (2011) Mesoporous Alumina-Supported Amines as Potential Steam-Stable Adsorbents for Capturing CO_2 from Simulated Flue Gas and Ambient Air, Energy Fuels 25:5528-5537.
[41] Sandhu NK, Pudasainee D, Sarkar P and Gupta R (2016) Steam Regeneration of Polyethylenimine-Impregnated Silica Sorbent for Postcombustion CO_2 Capture: A Multicyclic Study, Ind Eng Chem Res 55:2210-2220.
[42] Fayaz M and Sayari A (2017) Long-Term Effect of Steam Exposure on CO_2 Capture Performance of Amine-Grafted Silica, ACS Appl Mater Interfaces 9:43747-43754.
[43] Wilfong WC, Kail BW and Gray ML (2015) Rapid Screening of Immobilized Amine CO_2 Sorbents for Steam Stability by Their Direct Contact with Liquid H_2O, ChemSusChem 8:2041-2045.
[44] Min K, Choi W, Choi M (2017) Macroporous Silica with Thick Framework for Steam-Stable and High-Performance Poly(ethyleneimine)/Silica CO_2 Adsorbent, ChemSusChem 10:2518-2526.
[45] Potter ME, Cho KM, Lee JJ and Jones CW (2017) Role of Alumina Basicity in CO_2 Uptake in 3-Aminopropylsilyl-Grafted Alumina Adsorbents, ChemSusChem 10: 2192-2201.
[46] Sievers C, Noda Y, Qi L, Albuquerque EM, Rioux RM and Scott SL (2016) Phenomena Affecting Catalytic Reactions at Solid–Liquid Interfaces, ACS Catal 6:8286-8307.
[47] Ciftci A, Peng B, Jentys A, Lercher JA and Hensen EJM (2012) Support effects in the aqueous phase reforming of glycerol over supported platinum catalysts, Appl Catal A Gen 431-432:113-119.
[48] Lukens WW, Schmidt-Winkel P, Zhao D, Feng J and Stucky GD (1999) Evaluating Pore Sizes in Mesoporous Materials: A Simplified Standard Adsorption Method and a Simplified Broekhoff−de Boer Method, Langmuir 15:5403-5409.
[49] Bali S, Chen TT, Chaikittisilp W and Jones CW (2013) Oxidative Stability of Amino Polymer–Alumina Hybrid Adsorbents for Carbon Dioxide Capture, Energy Fuels 27:1547-1554.
[50] Turek AM, Wachs IE and DeCanio E (1992) Acidic properties of alumina-supported metal oxide catalysts: an infrared spectroscopy study, J Phys Chem 96:5000-5007.
[51] Aravind PR, Mukundan P, Pillai PK and Warrier KGK (2006) Mesoporous silica–alumina aerogels with high thermal pore stability through hybrid sol–gel route followed by subcritical drying, Microporous Mesoporous Mater 96:14-20.

[52] Digne M, Sautet P, Raybaud P, Euzen P and Toulhaut H (2004) Use of DFT to achieve a rational understanding of acid–basic properties of γ-alumina surfaces, J Catal 226:54-68.
[53] Ravenelle RM, Copeland JR, Van Pelt AH, Crittenden JC and Sievers C (2012) Stability of Pt/γ-Al_2O_3 Catalysts in Model Biomass Solutions, Top Catal 55:162-174.
[54] Ravenelle RM, Copeland JR, Kim WG, Crittenden JC and Sievers C (2011) Structural Changes of γ-Al_2O_3-Supported Catalysts in Hot Liquid Water, ACS Catal 1:552-561.
[55] Koichumanova K, Vikla AKK, de Vlieger DJM, Seshan K, Mojet BL and LeffertsL (2013) Towards Stable Catalysts for Aqueous Phase Conversion of Ethylene Glycol for Renewable Hydrogen, ChemSusChem 6:1717-1723.
[56] Réocreux R, Jiang T, Iannuzzi M, Michel C and Sautet P (2018) Structuration and Dynamics of Interfacial Liquid Water at Hydrated γ-Alumina Determined by ab Initio Molecular Simulations: Implications for Nanoparticle Stability, ACS Appl Nano Mater 1:191-199.
[57] Holewinski A, Sakwa-Novak MA and Jones CW (2015) Linking CO_2 Sorption Performance to Polymer Morphology in Aminopolymer/Silica Composites through Neutron Scattering, J Am Chem Soc 137:11749-11759.